The X-ray structure of the FMN-binding protein AtHal3 provides the structural basis for the activity of a regulatory subunit involved in signal transduction

Armando Albert[1*†] Martín Martínez-Ripoll[1†], Ana Espinosa-Ruiz[2], Lynne Yenush[2], Francisco A Culiáñez-Macià[2] and Ramón Serrano[2]

Background: The *Arabidopsis thaliana HAL3* gene product encodes for an FMN-binding protein (AtHal3) that is related to plant growth and salt and osmotic tolerance. AtHal3 shows sequence homology to ScHal3, a regulatory subunit of the *Saccharomyces cerevisae* serine/threonine phosphatase PPz1. It has been proposed that AtHal3 and ScHal3 have similar roles in cellular physiology, as *Arabidopsis* transgenic plants that overexpress AtHal3 and yeast cells that overexpress ScHal3 display similar phenotypes of improved salt tolerance. The enzymatic activity of AtHal3 has not been investigated. However, the AtHal3 sequence is homologous to that of EpiD, a flavoprotein from *Staphylococcus epidermidis* that recognizes a peptidic substrate and subsequently catalyzes the α,β-dehydrogenation of its C-terminal cysteine residue.

Results: The X-ray structure of AtHal3 at 2 Å resolution reveals that the biological unit is a trimer. Each protomer adopts an α/β Rossmann fold consisting of a six-stranded parallel β sheet flanked by two layers of α helices. The FMN-binding site of AtHal3 contains all the structural requirements of the flavoenzymes that catalyze dehydrogenation reactions. Comparison of the amino acid sequences of AtHal3, ScHal3 and EpiD reveals that a significant number of residues involved in trimer formation, the active site, and FMN binding are conserved. This observation suggests that ScHal3 and EpiD might also be trimers, having a similar structure and function to AtHal3.

Conclusions: Structural comparisons of AtHal3 with other FMN-binding proteins show that AtHal3 defines a new subgroup of this protein family that is involved in signal transduction. Analysis of the structure of AtHal3 indicates that this protein is designed to interact with another cellular component and to subsequently catalyze the α,β-dehydrogenation of a peptidyl cysteine. Structural data from AtHal3, together with physiological and biochemical information from ScHal3 and EpiD, allow us to propose a model for the recognition and regulation of AtHal3/ScHal3 cellular partners.

Addresses: [1]Grupo de Cristalografía Macromolecular y Biología Estructural, Instituto de Química Física 'Rocasolano', Consejo Superior de Investigaciones Científicas, Serrano 119, E-28006 Madrid, Spain and [2]Instituto de Biología Molecular y Celular de Plantas, Universidad Politécnica de Valencia-Consejo Superior de Investigaciones Científicas, Camino de Vera s/n, E-46022 Valencia, Spain.

*Corresponding author.
E-mail: xalbert@iqfr.csic.es

†These authors contributed equally to this work.

Key words: cell growth, flavoprotein, protein crystallography, regulation, salt stress, signal transduction

Received: **19 May 2000**
Revisions requested: **20 June 2000**
Revisions received: **13 July 2000**
Accepted: **21 July 2000**

Published: **24 August 2000**

Structure 2000, **8**:961–969

0969-2126/00/$ – see front matter

Introduction

The *Arabidopsis thaliana HAL3* gene encodes for a flavin mononucleotide (FMN) binding protein (AtHal3) which upon over-expression in transgenic *Arabidopsis* plants produces an altered growth rate and improved salt and drought tolerance [1]. The amino acid sequence of AtHal3 shows homology to several other eukaryotic and prokaryotic proteins: the DFP family of prokaryotic flavoproteins involved in DNA synthesis [2]; the *Staphylococcus epidermidis* epidermin-modifying enzyme EpiD [3], an enzymatically well-characterized flavoprotein; a group of uncharacterized eukaryotic proteins from rice, mouse, humans, *Drosophila melanogaster* and *Caenorhabditis elegans* [1]; and the core domain of Hal3 from *Saccharomyces cerevisiae* (ScHal3) and *Candida tropicalis* [4,5].

The homology of AtHal3 to ScHal3 is of particular significance as it has been proposed that AtHal3 and this eukaryotic protein have a similar role in cellular physiology [1,6]. ScHal3 is a protein that regulates the PPz1 type 1 protein phosphatase via direct interaction [7]. Previous work has shown that PPz1 and ScHal3 have opposing pleiotropic effects on cell-wall stability, salt tolerance and cell-cycle progression [4,6–9]. However, neither the requirement for an FMN cofactor nor enzymatic activity has been reported for ScHal3.

Espinosa-Ruiz *et al.* [1] showed that the overexpression of AtHal3 in *A. thaliana* produces similar phenotypes to those previously reported for ScHal3 in yeast. In addition, the authors showed that overexpression of AtHal3 in a yeast

mutant lacking ScHal3 partially rescues the phenotypes of ScHal3. Taken together, this information suggests that the function of AtHal3 is conserved between yeast and plants.

In this work, we present the X-ray structure of AtHal3 at 2.0 Å resolution. The structure provides evidence that AtHal3 and its homologous proteins represent a new functional FMN-binding domain with a similar fold to those of unrelated families of flavoproteins. Structural data, together with previously reported physiological and biochemical information from other proteins with similar sequences, allow us to propose a model for the recognition and regulation of AtHal3/ScHal3 cellular partners.

Results and discussion

The X-ray structure of the FMN-binding protein AtHal3 was solved by single isomorphous replacement with anomalous scattering (SIRAS) at 2 Å resolution (see Table 1 and Materials and methods section).

Table 1

Data collection, structure solution and refinement statistics.

	Native	$AuK(CN)_2$ derivative
Data collection		
Space group	$P6_3$	$P6_3$
Unit cell (Å)	112.31, 112.31, 33.18	111.96, 111.96, 32.93
Resolution limits (Å)	24.6 (2.0)	8.2 (2.6)
I/σ(I)	5.6 (1.8)	4.4 (1.8)
R_{merge} (%)*	9.1 (40.4)	15.5 (42.3)
Completeness (%)	97.1 (90.5)	96.8 (90.5)
Multiplicity	2.9 (2.7)	5.4 (4.8)
Temp (K)	120	120
Structure solution		
Number of sites	Reference	5
R_{Cullis} (c/a/anom)†	Reference	0.67/0.63/0.90
Phasing power (c/a/anom)‡	Reference	1.40/2.11/0.92
Mean FOM (c/a)§		0.34/0.18
Refinement		
Resolution range (Å)	12.0–2.0	
R factor	21.0 (25.6)	
R_{free}	26.3 (24.4)	
Number of atoms	1543	
Number of reflections	16,138	
Model		
amino acids	185	
water molecules	92	
FMN	1	
β-ME	1	
Ni	1	
Ramachandran plot residues in generously allowed regions	Lys19, Lys171, Gln200, Ala201	

*$R_{merge} = \Sigma_{hkl}\Sigma i|I_{hkl} - I_{hkl}|/\Sigma_{hkl}I_{hkl}$ for overall resolution range and the resolution shell from 2.1–2.0 Å. †$R_{Cullis} = \Sigma[|F_H| - (|F_{PH} - F_P|)]/\Sigma|F_H|$ for centric (c), acentric (a), and anomalous (anom) reflections. ‡Phasing power = mean value of the heavy-atom structure-factor amplitudes divided by the residual lack of closure. §FOM, figure of merit. Values in parentheses are for the highest resolution shell: 2.1–2.0 Å for native data and 2.75–2.6 Å for the derivative. β-ME, β-mercaptoethanol. The native structure is taken as a reference for the values given for the $AuK(CN)_2$ derivative.

Description of the structure

AtHal3 is a trimer with a threefold symmetry axis coincident with the crystallographic threefold axis (Figure 1). Hence, only a peptidic subunit is found for each asymmetric unit. The trimer can be described as a flattened triangular prism with a width of ~66 Å side and height of ~25 Å. Approximately 25% of the residues and the FMN groups in each protomer are involved in trimer formation (Figure 2) [10]. There is a 17.8% decrease of the solvent-accessible surface area per protomer on trimerization (the total accessible surface of a protomer is 7846 $Å^2$ and 1398 $Å^2$ of this area becomes buried on trimerization; see Materials and methods section). This value is in agreement with those calculated for molecules of similar molecular weight that form biological homodimers [10]. Gel-filtration chromatography experiments show that AtHal3 is also a trimer in solution (see Materials and methods section).

Figure 3 illustrates the three-dimensional structure of one AtHal3 subunit. AtHal3 is an α/β protein consisting of a six-stranded parallel β sheet sandwiched between two layers of α helices (Figure 3). In order to find similar structures to AtHal3, the atomic coordinates were submitted to the DALI server [11]. This server automatically compares

Figure 1

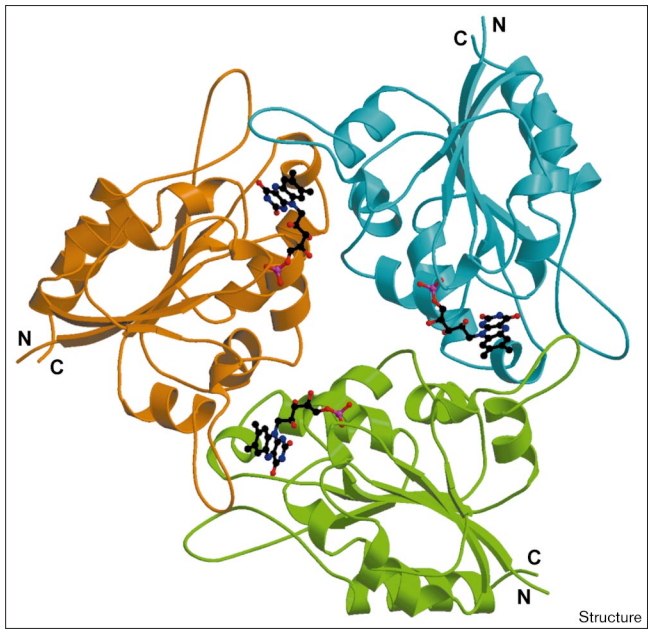

Ribbon representation of the AtHal3 structure viewed along the threefold axis defining the trimer. Each protomer is shown in a different color; the N and C termini are labeled. FMN groups are displayed in ball-and-stick mode.

Figure 2

Alignment comparing the amino acid sequences of AtHal3, the core domain of ScHal3 and EpiD. The alignment of AtHal3 and the core domain of ScHal3 is taken from [1] where all the homologous proteins belonging to eukaryotic organisms are aligned. The positions of the AtHal3 secondary structure elements determined from the crystal structure are shown above the AtHal3 sequence: β strands are shown as blue arrows and α helices as yellow rectangles. Residues that are identical in all sequences are shown in red. Residues involved in AtHal3 trimer formation are enclosed in green boxes (residues involved in trimerization are defined as those residues with an accessible surface area that decreases by >1 Å^2 upon trimer formation in AtHal3). Black dots, shown under the EpiD sequence, denote residues in AtHal3 with a surface area that decreases by >1 Å^2 owing to the presence of the FMN group. Hydrogen bonds between the FMN group and protein residues are shown as triangles (the blue triangle denotes a hydrogen bond to a residue of an adjacent protomer).

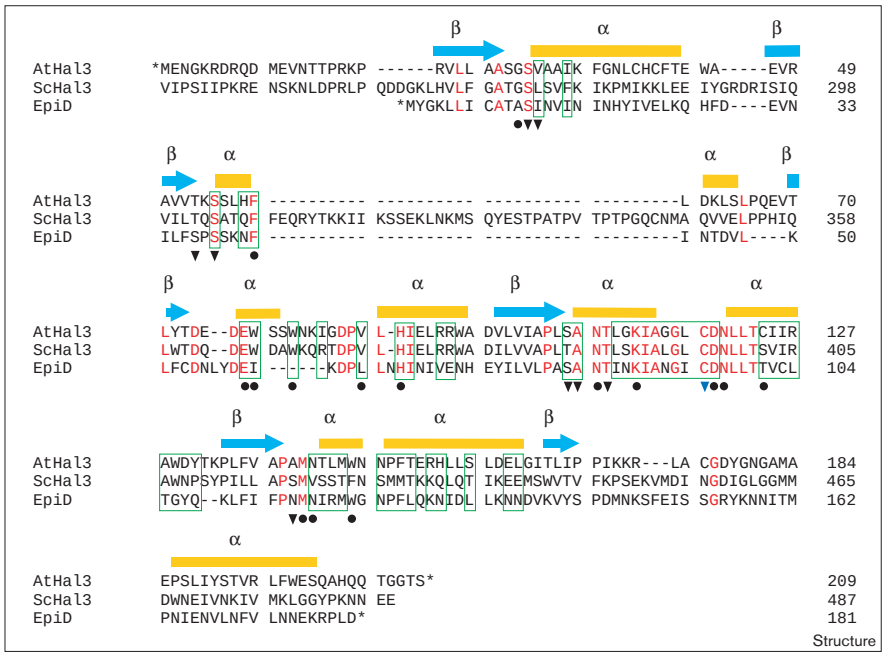

a query structure with those available in the Protein Data Bank (PDB) [12]. Nine of the ten best fits to the AtHal3 structure corresponded to NAD(P)-binding Rossmann-fold domains, and the remaining one corresponded to a flavodoxin-like domain [13].

A systematic study of the SCOP database [13] revealed that FMN-binding proteins exhibit one of four folds: the β/α (TIM)-barrel fold; the flavodoxin-like fold; the pyridoxine 5′-phosphate (PNP) oxidase-like β-barrel fold; or the α + β NADH oxidase/flavin reductase fold. As mentioned above, the AtHal3 fold is topologically similar to that of flavodoxin [14]. There are, however, several structural differences between them (Figures 3b and 4a). First, the central β sheet of AtHal3 is constructed with six strands ordered 321456, whereas that of flavodoxin consists of five β strands ordered 21345. Second, only 47 Cα atoms of AtHal3 present structural equivalents in flavodoxin (root mean squared deviation [rmsd] of 1.1 Å, with a criteria of 2.0 Å for considering atoms to be aligned; for 72 Cα atoms with a criteria of 3.0 Å the rmsd was 1.7 Å; see Materials and methods section). Third, the FMN group binds to a different site on each protein. Finally, AtHal3 is trimeric whereas flavodoxin is monomeric; none of the equivalent residues in AtHal3 and flavodoxin belongs to the helices involved in AtHal3 trimerization (i.e., α3a, α3b, α4a and α4b). In addition, AtHal3 and flavodoxin do not exhibit any sequence similarity, not even in residues involved in FMN binding (data not shown). Hence, we propose that AtHal3 defines a new subgroup of the family of FMN-binding proteins.

The AtHal3 structure was also compared with all known flavin adenine dinucleotide (FAD) binding folds, because this cofactor contains the entire FMN moiety. As with the FMN-binding proteins, the structural repertoire of the FAD-binding proteins is quite diverse and includes proteins belonging to the all-α class, α/β class, α + β class, and all-β class [13]. Our study revealed that the middle domain of pyruvate oxidase [15] and AtHal3 present the same overall topology (α/β class, deoxyhypusine synthase (DHS) like NAD/FAD-binding domain fold [13]; Figure 4b). As in the case of flavodoxin, however, the AtHal3 residues that belong to helices involved in trimerization do not have structural equivalents in pyruvate oxidase (using a criteria of 2.0 Å, 43 Cα atoms of AtHal3 align with structural equivalents in pyruvate oxidase with an rmsd of 1.0 Å; if the criteria is 3.0 Å, 64 Cα atoms align with an rmsd of 1.8 Å). Remarkably, the FMN PO_4 moiety of AtHal3 and the FAD PO_4 moiety of pyruvate oxidase are structurally equivalent. On the other hand, the ribitol and isoalloxazine moieties are bound to the proteins in opposite directions.

As shown previously [1] and in this article, AtHal3 presents different structural and functional properties to flavodoxin and pyruvate oxidase. It is interesting to note, however, that AtHal3 adopts a similar fold to these unrelated families of flavoproteins.

The FMN-binding site

The FMN group is located at the interface between two adjacent protomers (Figure 1). The aromatic isoalloxazine

Figure 3

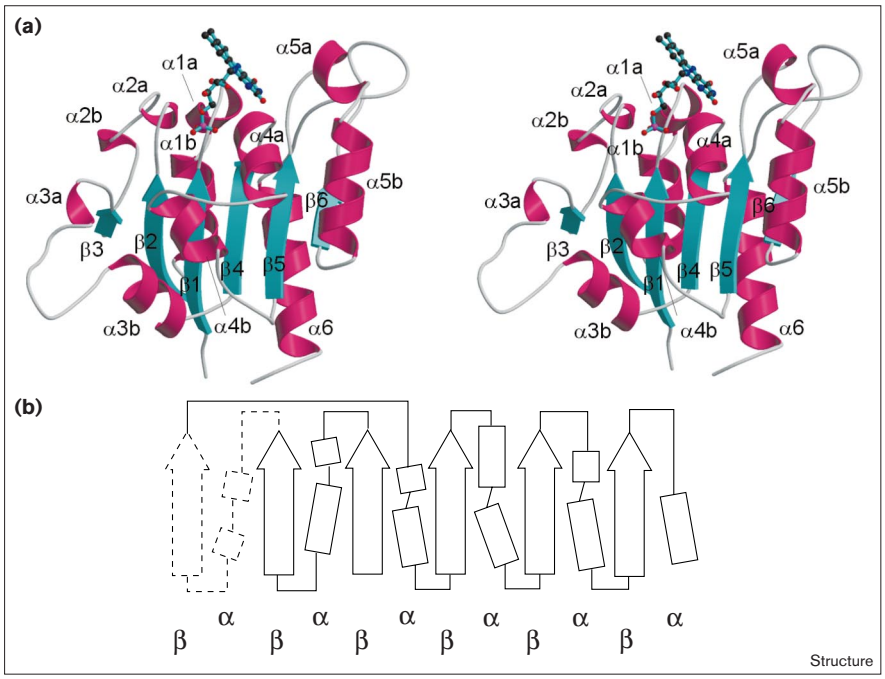

Protein fold and topology of AtHal3. **(a)** Stereoview ribbon representation of the AtHal3 protomer showing the secondary structural elements. α Helices are colored magenta and β strands cyan. The FMN group is displayed in ball-and-stick mode. **(b)** A topological diagram of the AtHal3 structure: β strands are shown as arrows and α helices as rectangles. Secondary structure elements that are not conserved in other proteins with the flavodoxin-like fold are depicted with dashed lines (see text).

moiety is placed in a hydrophobic pocket constructed from residues of two adjacent subunits (Figure 5a), although all the hydrogen bonds between the protein and isoalloxazine are made with one subunit. Interestingly, SerA29 OG and AlaA107 N, which hydrogen bond to the isoalloxazine N3 and O2 atoms, respectively, are conserved in AtHal3-related proteins (Figure 2). AlaA107 NH, at the N terminus of the α4a helix, provides the positively charged environment of the N1–C2 = O2 locus found in flavoenzymes that catalyze a dehydrogenation reaction [16] (Figure 5a). The isoalloxazine N5 atom is not hydrogen bonded to any protein donor, as in vanillyl-alcohol oxidase [17] and glycolate oxidase [18]. These enzymes exhibit a relatively high (> –25 mV) redox potential. It has been proposed that the hydrogen bond to N5 destabilizes the protonated reduced cofactor, hence decreasing the oxidative power of the cofactor [16]. It is also known that the reduction of the FMN group is hindered by the presence of negatively charged residues in the FMN-binding site or by coplanar aromatic π–π interactions between aromatic residues and the isoalloxazine moiety of the FMN group [19]. Neither negatively charged residues nor π–π stacking interactions are found around the isoalloxazine ring in AtHal3. On the contrary, three T-type aromatic interactions [20], between the aromatic moiety of the FMN group and PheA59, TrpB78 and TrpB81, will stabilize a reduced intermediate (Figure 5b). The *re* side of the isoalloxazine ring defines a small cavity made up primarily of hydrophobic residues with the exception of a diad, HisB90–GluB77 (Figure 5b). The accessible volume of this cavity is defined by a system of four water molecules located in a plane 3.7 Å above the *re* side of the isoalloxazine ring. This water system is flanked by loops connecting β5 with α5a, α4a with α4b and by the His90–Glu77 diad. These facts together with the structural relationship between the FMN-binding site AtHal3 and the flavin-dependent dehydrogenases, indicates that AtHal3 should be a functional redox flavoenzyme and that the cavity at the *re* side of the isoalloxazine ring defines the active site.

The phosphate and ribitol moieties of FMN are hydrogen bonded mainly to residues that belong to one AtHal3 subunit. Among them, GlyA28, SerA55, ThrA109 and CysB118 are conserved in AtHal3-related proteins. ThrA53 and SerA106 align with a threonine or a serine residue in ScHal3 and EpiD, respectively (Figure 2). Both AtHal3 and pyruvate oxidase use the polarity provided by the N terminus of the small α2a helix to bind the PO_4 moiety (Figure 4b). ThrA53 at the end of this helix is a conserved residue and structurally equivalent in both enzymes. On the other hand, flavodoxin uses the polarity of the N terminus of α1 to bind the FMN PO_4 moiety (Figure 4a). Despite the large number of polar groups in the ribitol moiety, only two ribitol hydroxyl groups are hydrogen bonded to the protein.

Description of the molecular surface

Each lateral side of the trimer defines an elongated groove, capped by a mobile flap (residues Lys171–Ala182),

Figure 4

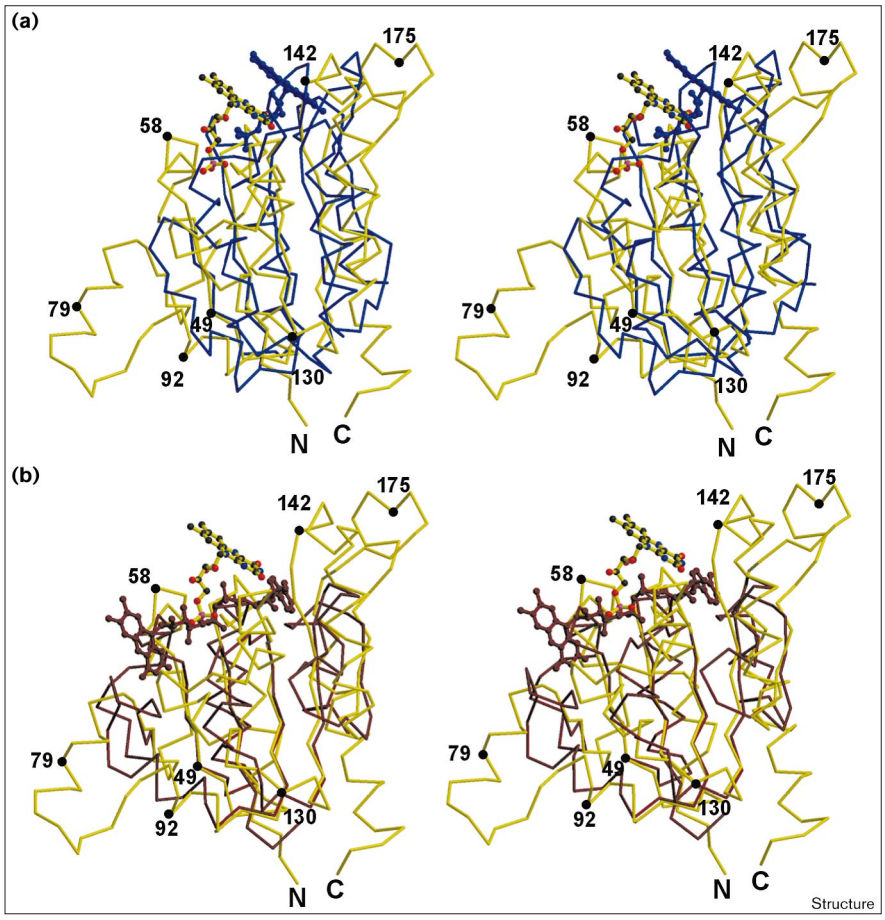

Stereoview Cα traces for the aligned structures of **(a)** AtHal3 (yellow) and flavodoxin (blue), and **(b)** AtHal3 (yellow) and pyruvate oxidase (red). The FMN and FAD groups are displayed in ball-and-stick mode. Atoms belonging to AtHal3 FMN are shown in CPK colors. The coordinates of flavodoxin and pyruvate oxidase were obtained from the PDB (entry codes 2FX2 and 1POX, respectively).

with an entrance to the active site. The reactivity of the active site and the groove is apparent from the fact that $[Au(CN)_2]^-$ complexes fill these cavities when crystals are soaked to prepare the heavy-atom derivative.

The electrostatic charge potential at the molecular surface of the trimer produces an intrinsic dipolar moment in the direction of the central threefold axis (see Materials and methods section). This is a consequence of the apposite charge distributions on both sides of the trimer. The acidic side displays a cavity partially filled by a metal atom lying at the threefold axis. The electron-density map at this site shows this atom to be octahedrally coordinated to six water molecules, suggesting a high affinity for metals at this site. Neither the presence of the metal site nor a functional role has been reported for any of the AtHal3-related proteins. Total reflection fluorescence techniques (see Materials and methods section) were used to identify the chemical nature of this metal atom. The results are consistent with one nickel atom per trimer. The purification step using nickel-binding affinity chromatography (see Materials and methods section) can explain the source of this atom; hence, the metal site observed in the electron-density map was assigned as a nickel atom for further structure refinement.

Comparison of AtHal3 with the homologous protein EpiD

The enzymatic activity of AtHal3 and ScHal3 has not been reported. There is, however, a striking sequence similarity between the FMN-dependent EpiD protein and AtHal3 (Figure 2). EpiD is a flavoprotein involved in the maturation of the peptidic lantibiotic epidermine [3,21]. EpiD specifically recognizes the gene product EpiA, the peptidic precursor of epidermine, and subsequently catalyzes an α,β-dehydrogenation of the EpiA C-terminal cysteine residue.

A significant number of AtHal3 residues involved in trimer formation and FMN-binding are conserved, or display a conservative change, in ScHal3 (percentage identity 38.3%; percentage similarity 75.0%) and in EpiD (38.3% and 66.7%; Figure 2). Hence, we propose that ScHal3 and EpiD should form trimers, having similar structures and functions to AtHal3.

Figure 5

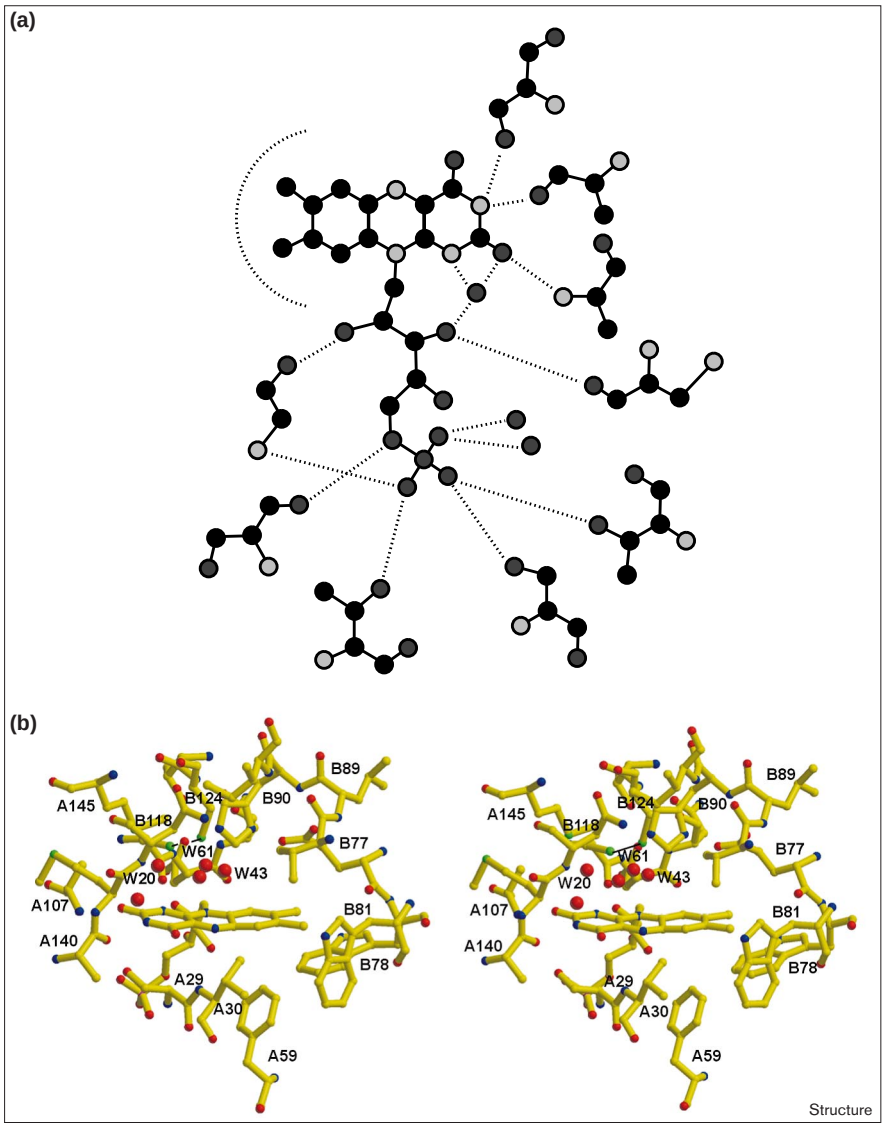

Protein and solvent interactions with the FMN group. **(a)** Schematic representation of the AtHal3–FMN interactions, identifying residues involved in hydrogen bonding to the cofactor. Hydrophobic interactions between the aromatic moiety of the isoalloxazine ring and AtHal3 are also displayed. Distances are indicated in Å. Residues are labeled using the three-letter amino acid code and the letters A and B are used to denote the different subunits of the trimer. **(b)** Stereoview of the FMN environment. Atoms are shown in standard colors; water molecules are displayed as red spheres.

Several structural features suggest that AtHal3 might catalyze the α,β-dehydrogenation of a peptidyl cysteine residue as does EpiD. First, a cysteine sidechain fits perfectly into the accessible volume of the active site (Figure 6a). Second Fraaije and Mattevi [16] revealed that flavoenzymes that catalyze a substrate dehydrogenation show a striking similarity in the position of the ligand atoms being dehydrogenated by the flavin group. The site of the oxidative attack typically binds in front of the flavin N5 and an adjacent group is also required to facilitate the formation of a double bond in the oxidized product. In AtHal3, the system of water molecules that define a plane above the *re* side of the FMN group mimics the position of a peptidyl cysteine substrate according to the structural analysis presented by Fraaije and Mattevi [16] (Figures 5b and 6b). Water molecule W43, above flavin N5, is located where the oxidative attack would take place and mimics the CA atom of the peptidyl cysteine. Water molecules W20 and W61 would correspond to the positions of the SG and the CB atoms of the cysteine sidechain, respectively. In this situation, the thiol group (W20 in the crystal structure) would be activated by two hydrogen bonds formed to AsnA142 NH and the N3 atom of FMN. Consequently, the acidity of the hydrogen atoms of the adjacent CB atom (W61 in the crystal structure) would be enhanced. One of these hydrogen atoms would be placed close to (~3 Å) the basic His90–Glu77 diad (Figure 6b). Similar geometrical constraints can be found in the active site of the acyl-CoA dehydrogenase; in this enzyme, a concerted α,β-dehydrogenation of the substrate is proposed [22–24]. Hence, a similar reaction mechanism might occur in AtHal3. This

Figure 6

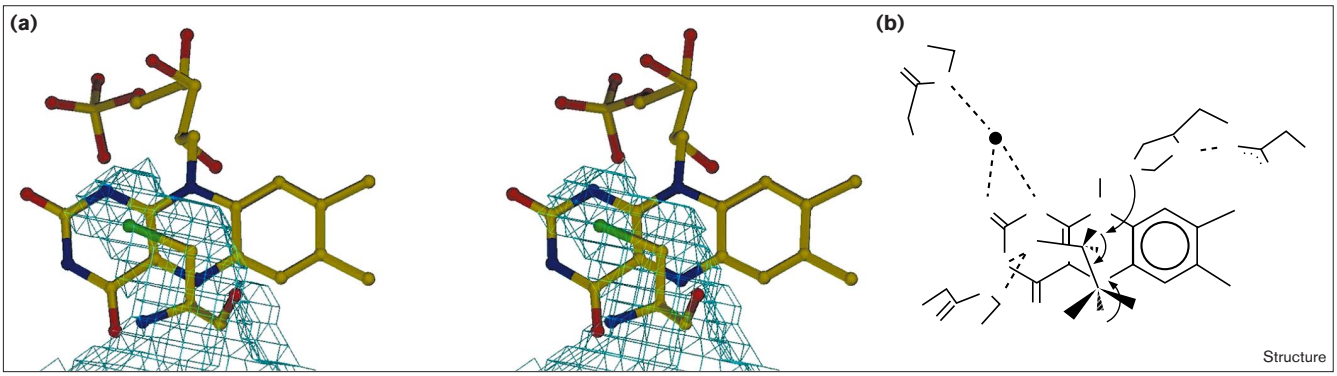

The AtHal3 active site. **(a)** Stereoview detail of the molecular surface using a probe of 1.4 Å [39]. A peptidyl cysteine residue is modeled inside the cavity. **(b)** Proposed mechanism for the α,β-dehydrogenation of a peptidyl cysteine residue in the active site of AtHal3.

would imply the transfer of one proton from CB to the His90–Glu77 diad followed by the expulsion of hydride from the CA to the N5 atom of FMN (Figure 6b). The subsequent reoxidation of the FMN group could be achieved by the direct interaction of molecular oxygen with the water-accessible O4 atom of FMN. The exact match of the peptidyl cysteine sidechain with the narrow active-site cavity (Figure 6a) would cause the system of water molecules to be expelled upon substrate binding. This will shield the reaction cavity from the solvent as in other flavoenzymes [16]. A peptidyl serine would also fit in the active site of AtHal3. However, the larger electronegative value of oxygen with respect to that of sulfur explains why the oxidation of a peptidyl serine is not likely to be catalyzed. From a thermodynamic point of view, the affinity of a hydroxyl group for the active site NH groups is reduced when compared with that of a thiol group. From the kinetic point of view, a sulfur atom hydrogen bonded to NH groups would be more activated than an oxygen atom; consequently, in the case of a cysteine residue, the hydrogen atoms bound to CB would be more acidic than with a serine residue.

As mentioned above, the active site is accessible from the center of an elongated groove located on the lateral side of the trimer. It is tempting to speculate that this groove would recognize a specific sequence of the peptidic cellular partner of AtHal3.

Regulatory activity of AtHal3

It has been proposed that ScHal3 and AtHal3 have a similar role in cellular physiology, regulating pathways related to the cell cycle and salt and osmotic stress [1,7]. The cellular partner of AtHal3 has not been identified. In *S. cerevisiae*, however, de Nadal *et al.* [7] demonstrated that the homologous protein ScHal3 is a regulatory subunit of the protein phosphatase PPz1.

de Nadal *et al.* [7] propose that the regulation of PPz1 by ScHal3 can be explained through direct interaction between ScHal3 and the PPz1 C-terminal domain, resulting in inactivation of the phosphatase. However, this model may be oversimplified. For example, *in vitro* the interaction of ScHal3 with PPz1 is hindered by the functional N-terminal domain of PPz1 [7]. In addition, it is not known whether the ScHal3–PPz1 interaction is constitutive or modulated by stress. It is possible that the interaction is constitutive and that stress triggers the enzymatic activity of ScHal3, in turn modulating phosphatase activity. Future experiments will investigate the mechanism of regulation of PPz1 by ScHal3.

Our work shows that AtHal3 has an intrinsic dipole moment coincident with the threefold axis that defines the trimer. The dipolar moment ensures a directionality in the possible interaction with another cellular component. It is interesting that this dipole seems to be unrelated to the redox activity as the active site is accessible on the lateral side of the trimer. On the contrary, the intrinsic dipole moment reported for flavodoxin and the flavodoxin-like FMN-binding domain of human cytochrome P450 [25] ensures an approach of its partner to the FMN group. Hence, it seems that AtHal3 and the central domain of ScHal3 are designed to have a dual activity: first interacting with their molecular partner and then undergoing a redox reaction. It is tempting to speculate that this dual activity could be related to a novel selective regulatory mechanism that responds to the cellular environment.

Currently we are working on the crystallization of the AtHal3–Ppz1 and ScHal3–PPz1 complexes. The X-ray structure of these complexes, together with complementation studies of AtHal3 and ScHal3 mutants in the *S. cerevisiae* model system, will help us to understand crucial aspects of the mode of regulation of AtHal3 and ScHal3.

Of particular interest are mutations of the catalytic residue His90 in AtHal3 and ScHal3, which is likely to abolish redox activity of these enzymes, and of some key residues on the surface of the trimer that would modulate the interaction with PPz1.

Biological implications

The progressive salinization of irrigated land in semi-arid regions has exposed plants to high salt concentrations. Plant molecular biologists have made great efforts to identify and elucidate the underlying mechanism that governs salt stress responses in order to engineer crop plants with greater salt tolerance [26]. The *Arabidopsis thaliana* protein AtHal3 is of interest to such studies as it is known to have a role in plant growth and salt and osmotic tolerance. AtHal3 was first characterized owing to its sequence homology with *Saccharomyces cerevisiae* Hal3 (ScHal3), a protein that regulates the PPz1 type 1 protein phosphatase via direct interaction [7]. Previous work [4,8] has shown that yeast cells that overexpress ScHal3 or lack PPz1 display increased resistance to sodium and lithium. Three lines of evidence [1] suggest that the function of AtHal3 is conserved between yeast, plants and other eukaryotic organisms: transgenic *Arabidopsis* plants that overexpress AtHal3 display altered growth and osmoresistance phenotypes, similar to those observed in yeast cells that overexpress ScHal3; the overexpression of AtHal3 in a yeast mutant lacking ScHal3 partially rescues the phenotypes of ScHal3; and the AtHal3 sequence is conserved in a group of uncharacterized eukaryotic proteins. In addition, it has been demonstrated that AtHal3 contains a non-covalently bound FMN group. The fact that AtHal3 is a flavoprotein suggested that a redox process is also involved in the regulation of its cellular partner.

The analysis of the structure of AtHal3 suggests that this protein has a dual activity: the protein first interacts with its cellular partner and then catalyzes the α,β-dehydrogenation of a peptidyl cysteine. This dual activity could be related to a novel selective regulatory mechanism that responds to the cellular environment. The effect of AtHal3 and ScHal3 on cell growth and salt tolerance may represent the existence of a link between certain environmental conditions and the decision to progress through a new cell cycle. Our findings provide the structural basis for the recognition and regulation of the cellular partner for AtHal3-related proteins. The combination of structural and mutagenic analysis of AtHal3 might contribute to the generation of salt-tolerant crops — a challenge for modern plant biotechnology.

Materials and methods

AtHal3 was expressed and purified as described by Espinosa-Ruiz *et al.* [1]. The protein was concentrated to 10 mg/ml in buffer comprising 0.1 M Tris-HCl pH 7.5, 0.1 M imidazole and 5 mM β-mercaptoethanol. Experiments were carried out at room temperature. Crystals were grown by vapour diffusion from drops containing AtHal3 and reservoir solutions (0.1 M Tris-HCl pH 7, 2.5 M ammonium sulfate) in a 2:1 ratio. For data collection, crystals were flash-cooled at 120K from a solution containing mother liquor plus 20% glycerol. The crystal structure of AtHal3 was solved by single isomorphous replacement using the anomalous information corresponding to one wavelength for one gold derivative (see Table 1). X-ray data from native and derivative were collected using CuKα radiation on an in-house source (Mar 345 image-plate detector on Enraf Nonius rotating-anode generator). Friedel pairs for the derivative were also collected. The data were processed using MOSFLM [27] in space group $P6_3$. The coordinates of one site from the gold di-cyano aurate derivative were determined using the Patterson interpretation routine of SHELX [28]. All other sites were obtained by difference Fourier techniques. All calculations were performed using programs of the CCP4 package [29] and the final refinement and solvent-flattening were performed using SHARP [30]. The resulting experimental electron-density map was of good quality and unambiguously allowed the tracing of a polypeptide chain for AtHal3 using the program O [31]. The electron density was of poor quality for residues 173–179 and these were modeled; no density was visible for residues 1–17 and 203–209. The initial model was refined first using the simulated annealing routine of X-PLOR [32]. Several cycles of restrained refinement at 2.0 Å resolution using REFMAC [33] followed by interactive model building were carried out (see Table 1). The final electron-density map for FMN is shown in Figure 7. The stereochemistry of the model was verified with PROCHECK [34]. Ribbon figures were produced using MOLSCRIPT [35], RASTER 3D [36] and O [31]. The accessible surface area of the AtHal3 trimer and protomer, and the electrostatic potential on the molecular surface of AtHal3 were calculated with GRASP [37]. Rigid-body superposition calculations were performed with MNYFIT [38]. The identification of the nickel atom in AtHal3 was carried out by total reflection fluorescence techniques at Servicio Interdisciplinar de Investigación (SIDI) at Universidad Autónoma de Madrid. A 600 μg sample of AtHal3 diluted in 60 μl of 0.01 M Tris-HCl pH 7.5, 0.1 M imidazole, 5 mM β-mercaptoethanol was used in the analysis. The nickel concentration of the sample was related to the known concentration of sulfur atoms. The procedure yielded 0.92 nickel atoms per trimer of AtHal3. The characterization of the oligomeric character of the native enzyme in solution was performed using gel-filtration chromatography. Approximately 50 μg of pure AtHal3 and 50 μg of bovine serum albumin (BSA) were fractionated on

Figure 7

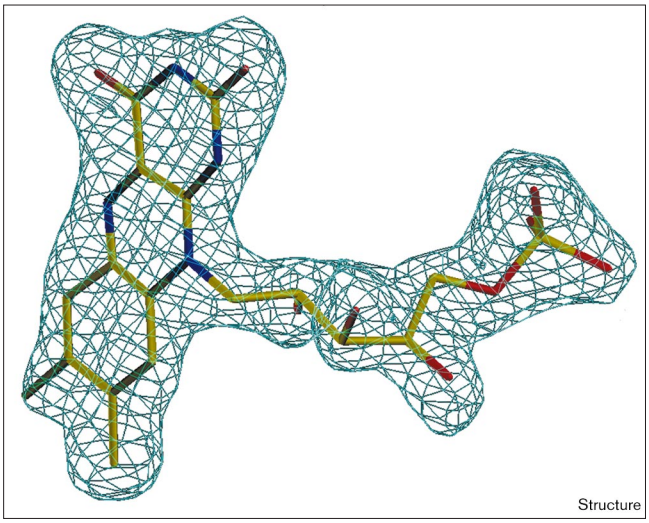

Final electron-density map for FMN contoured at 1σ.

a Superdex HR 10/30 column (Amersham Pharmacia). Both proteins eluted in the same fractions, approximately at 58% of the bed solvent volume (molecular weight of BSA is 68 kDa, estimated molecular weight for the AtHal3 trimer 69 kDa). Sodium dodecyl sulfate polyacrylamide gel electrophoresis showed two bands, one corresponding to the molecular weight of BSA and the other corresponding to the molecular weight of the AtHal3 protomer (23 kDa).

Accession numbers

The coordinates and structure factors amplitudes of AtHal3 have been deposited in the PDB (accession code 1E20).

Acknowledgements

We thank J Hermoso and R Sánchez-Diaz for their helpful suggestions. LY holds an International Research Fellow Award of the National Science Foundation (USA). This work was supported by grants of the Spanish Ministerio de Educación y Cultura (PB98-0565-C04-04, PB98-0565-C04-03 and PB98-0565-C04-01).

References

1. Espinosa-Ruiz, A., Belles, J.M., Serrano, R. & Culiañez-Macia, F.A. (1999). *Arabidopsis thaliana* AtHAL3: a flavoprotein related to salt and osmotic tolerance and plant growth. *Plant J.* **20**, 529-539.
2. Spitzer, E.D. & Weiss, B. (1985). *dfp* gene of *Escherichia coli* K-12, a locus affecting DNA-synthesis codes for a flavoprotein. *J. Bacteriol.* **164**, 994-1003.
3. Kupke, T., Stevanovic, S., Sahl, H.G. & Götz, F. (1992). Purification and characterization of EpiD, a flavoprotein involved in the biosynthesis of the lantibiotic epidermin. *J. Bacteriol.* **174**, 5354-5361.
4. Ferrando, A., Kron, S.J., Rios, G., Fink, G.R. & Serrano, R. (1995). Regulation of cation-transport in *Saccharomyces cerevisiae* by the salt tolerance gene HAL3. *Mol. Cell Biol.* **15**, 5470-5481.
5 Rodriguez, P.L., Ali, R. & Serrano, R. (1996). CtCdc55p and CtHa13p: two putative regulatory proteins from *Candida tropicalis* with long acidic domains. *Yeast* **12**, 1321-1329.
6. Clotet, J., Gari, E., Aldea, M. & Ariño, J. (1999). The yeast Ser/Thr phosphatases Sit4 and Ppz1 play opposite roles in regulation of the cell cycle. *Mol. Cell Biol.* **19**, 2408-2415.
7. de Nadal, E., Clotet, J., Posas, F., Serrano, R., Gómez, N. & Ariño, J. (1998). The yeast halotolerance determinant Hal3p is an inhibitory subunit of the Ppz1p Ser/Thr protein phosphatase. *Proc. Natl Acad. Sci. USA* **95**, 7357-7362.
8. Posas, F., Bollen, M., Stalmans, W. & Ariño, J. (1995). Biochemical characterization of recombinant yeast PPZ1, a protein phosphatase involved in salt tolerance. *FEBS Lett.* **368**, 39-44.
9. Lee, K.S., Hines, L.K. & Levin, D.E. (1993). A pair of functionally redundant yeast genes (PPZ1 and PPZ2) encoding type1-related protein phosphatases function within the PKC1-mediated pathway. *Mol. Cell Biol.* **13**, 5843-5853.
10. Jones, S. & Thornton, J.M. (1996). Principles of protein–protein interaction. *Proc. Natl Acad. Sci USA* **93**, 13-20.
11. Holm, L. & Sander, C. (1998). Touring protein fold space with Dali/FSSP. *Nucleic Acids Res.* **26**, 316-319.
12. Berman, H.M., *et al.*, & Bourne, P.E. (2000). The Protein Data Bank. *Nucleic Acids Res.*, **28**, 235-242.
13. Murzin, A.G., Brenner, S.E., Hubbard, T. & Chothia, C. (1995). SCOP: a structural classification of proteins database for the investigation of sequences and structures. *J. Mol. Biol.* **247**, 536-540.
14. Watenpaugh, K.D., Sieker, L.C., Jensen, L.H., Legall, J. & Dubourdieu, M. (1972). Structure of the oxidized form of a flavodoxin at 2.5 Å resolution. Resolution of the phase ambiguity by anomalous scattering. *Proc. Natl Acad. Sci. USA* **69**, 3185-3188.
15. Muller, Y.A. & Schulz, G.E. (1993). Structure of the thiamine- and flavin-dependent enzyme pyruvate oxidase. *Science* **259**, 965-967.
16. Fraaije, M.W. & Mattevi, A. (2000). Flavoenzymes: diverse catalysts with recurrent features. *Trends Biochem. Sci.* **25**, 126-132.
17. Fraaije, M.W., van den Heuvel, R.H., van Berkel, W.J. & Mattevi, A. (1999). Covalent flavinylation is essential for efficient redox catalysis in vanillyl-alcohol oxidase. *J. Biol. Chem.* **274**, 35514-35520.
18. Lindqvist, Y. (1989). Refined structure of spinach glycolate oxidase at 2 Å resolution. *J. Mol. Biol.* **209**, 151-166.
19. Zhou, Z. & Swenson, R.P. (1996). The cumulative electrostatic effect of aromatic stacking interactions and the negative electrostatic environment of the flavin mononucleotide binding site is a major determinant of the reduction potential for the flavodoxin from *Desulfovibrio vulgaris*. *Biochemistry* **50**, 15980-15988.
20. Burley, S.K. & Petsko, G.A. (1988). Weakly polar interactions in proteins. In *Advances in Protein Chemistry.* (Anfinsen, C.B., Edsall, J.T., Richards, F.M. & Eisenberg, D.S., eds), pp. 125-189, Academic Press, Inc., New York.
21. Kupke, T., Kempter, C., Gnau, V., Jung, G. & Gotz, F. (1994). Mass spectroscopic analysis of a novel enzymatic-reaction. Oxidative decarboxylation of the lantibiotic precursor peptide EpiA catalyzed by the flavoprotein EpiD. *J. Biol. Chem.* **269**, 5653-5659.
22. Ghisla, S. & Massey, V. (1989). Mechanisms of flavoprotein-catalyzed reactions. *Eur. J. Biochem.* **181**, 1-17.
23. Ghisla, S. (1984). Mechanisms of α,β-dehydrogenation of fatty acids CoA derivatives by flavin enzymes. In *Flavins and Flavoproteins* (Bray, R.C., Engel, P.C. & Mayhew, S.G., eds), pp. 385-401, W. de Gruyter, Berlin.
24. Schopfer, L.M., Massey, V., Ghisla, S. & Thorpe, C. (1988). Oxidation-reduction of general acyl-CoA dehydrogenase by the butyryl-CoA/crotonyl-CoA couple. A new investigation of the rapid reaction kinetics. *Biochemistry* **27**, 6599-6611.
25. Zhao, Q., *et al.*, & Driessen, H.P. (1999). Crystal structure of the FMN-binding domain of human cytochrome P450 reductase at 1.93 Å resolution. *Protein Sci.* **8**, 298-306.
26. Serrano, R. (1996). Salt tolerance in plants and microorganisms: toxicity targets and defense responses. *Int. Rev. Cytol.*, **165**, 1-52.
27. Leslie, A.G.W. (1987). MOSFLM. In *Proceedings of the CCP4 Study Weekend.* (Machin, J.R. & Papiz, M.Z., eds), pp. 39-50, SERC Daresbury Laboratory, Warrington, UK.
28. Sheldrick, G.M. (1991). The SHELXS system. In *Crystallographic Computing 5.* (Podjarny, P.D. & Thiery, J.D., eds), pp. 145-157. IUCR, Oxford University Press, Oxford.
29. Bailey, S. (1994). The CCP4 suite, programs for protein crystallography. *Acta Crystallogr. D* **50**, 760-763.
30. de la Fortelle, E. & Bricogne, G. (1997). Maximum-likelihood heavy-atom parameter refinement for multiple isomorphous replacement and multiwavelength anomalous diffraction methods. *Methods Enzymol.* **276**, 472-494.
31. Jones, T.A., Zou, J.Y., Cowan, S.W. & Kjeldgaard, M. (1991). Improved methods for model building in electron density maps and the location of errors in these models. *Acta Crystallogr. A* **47**, 110-119.
32. Brünger, A.T. (1988). Crystallographic refinement by simulated annealing application to a 2.8 Å resolution structure of aspartate-aminotransferase. *J. Mol. Biol.* **203**, 803-816.
33. Murshudov, G.N., Vagin, A.A. & Dodson, E.J. (1997). Refinement of macromolecular structures by the maximum-likelihood method. *Acta Crystallogr. D* **53**, 240-255.
34. Laskowski, R.A., MacArthur, M.W., Moss, D.S. & Thornton, J.M. (1993). PROCHECK, a program to check the stereochemical quality of protein structures. *J. Appl. Crystallogr.* **26**, 283-291.
35. Kraulis, P.J. (1991). MOLSCRIPT, a program to produce both detailed and schematic plots of protein structures. *J. Appl. Crystallogr.* **24**, 946-950.
36. Merritt, E.A. & Murphy, M.E.P. (1994). RASTER3D Version 2.0, a program for photorealistic molecular graphics. *Acta Crystallogr. D* **50**, 869-873.
37. Nicholls, A., Bhraradwaj, R. & Honig, B. (1993). GRASP: graphical representation and analysis of surface properties. *Biophys. J.* **64**, 166.
38. Sutcliffe, M.J., Haneef, I., Carney, D. & Blundell, T.L. (1987). Knowledge based modeling of proteins. 1. 3-dimensional frameworks derived from the simultaneous superposition of multiple structures. *Protein Eng.* **1**, 377-384.
39. Kleywegt, G.J. & Jones, T.A. (1994). Detection, delineation, measurement and display of cavities in macromolecular structures. *Acta Crystallogr. D* **50**, 178-185.

Because *Structure with Folding & Design* operates a 'Continuous Publication System' for Research Papers, this paper has been published on the internet before being printed (accessed from http://biomednet.com/cbiology/str). For further information, see the explanation on the contents page.